Journal of The Electrochemical Society, **156** (12) G206-G212 (2009)
0013-4651/2009/156(12)/G206/7/$25.00 © The Electrochemical Society

The Effect of Chemical Composition on the Structure and Dielectric Properties of the Columbites $A^{2+}Nb_2O_6$

Anatolii Belous,[a,z] Oleg Ovchar,[a,z] Bostjan Jancar,[b] Matjaz Spreitzer,[b] Giuseppe Annino,[c] Dmitrij Grebennikov,[d] and Peter Mascher[d,*]

[a] *V. I. Vernadskii Institute of General and Inorganic Chemistry, National Academy of Sciences of Ukraine, Kyiv 03680, Ukraine*
[b] *Jozef Stefan Institute, 1000 Ljubljana, Slovenia*
[c] *Istituto per i Processi Chimico-Fisici, Consiglio Nazionale delle Ricerche, 56124 Pisa, Italy*
[d] *Department of Engineering Physics and Centre for Emerging Device Technologies, McMaster University, Hamilton, Ontario L8S 4K1, Canada*

This paper summarizes the synthesis and properties of the materials based on the columbites $A^{2+}_{1+x}Nb_2O_{6+x}$ (A^{2+} = Mg, Co, Zn) in the vicinity of their stoichiometric composition. The evolution of the phase composition, microstructure, and microwave dielectric properties of the studied materials have been considered with respect to different sintering atmospheres (air and oxygen). The correlation between the data obtained by electron microscopy, positron lifetime spectroscopy, and microwave characterization at the frequencies of 10 and 50–70 GHz has been presented and discussed. The A-site deficiency ($x < 0$) always leads to the formation of the secondary Nb-rich phase in the columbite matrix, which significantly deteriorates the microwave quality factor (Q) of the sintered materials. In contrast, the Nb deficiency improves the microstructure of the ceramics but initiates the formation of A^{2+}-rich secondary phases. The competing effect of these factors results in the nonlinear variation $Q(x)$. The resulting magnitudes (Qxf) attain values of 100,000–120,000 GHz depending on the A^{2+} ion and sintering atmosphere.
 [DOI: 10.1149/1.3236661]

Manuscript submitted April 21, 2009; revised manuscript received July 28, 2009. Published October 12, 2009.

Binary niobates $A^{2+}Nb_2O_6$ (A^{2+} = Mg, Co, Zn) with the columbite structure exhibit excellent dielectric properties at microwave (MW) frequencies.[1-3] Moreover, they are generally used as precursor phases for the synthesis of complex perovskites including both the relaxors $Pb(A^{2+}_{1/3}Nb_{2/3})O_3$ [4] and the high Q dielectrics $Ba(A^{2+}_{1/3}Nb_{2/3})O_3$.[5] Even though the columbites demonstrate rather poor temperature coefficients of the resonant frequency (τ_f is around −70 ppm/C), their high quality factor (the product Qxf reaches 80,000–90,000 GHz in Mg- and Zn-containing materials[1,3]) together with the moderate dielectric constant (ε = 20–23) make them promising candidates for applications in MW engineering. This is particularly relevant with the current tendency to expand the operating frequency ranges of MW wireless communications toward the millimeter wavelength band, where materials with a moderate ε and extremely high Q are required.[6] However, the MW dielectric properties, especially the MW dielectric loss ($\tan\delta = 1/Q$), of the columbites are to a large extent sensitive to the precursors and the materials' processing.[3,4,7] For instance, changes in both starting reagents and sintering temperatures of the stoichiometric cobalt niobate ($CoNb_2O_6$) have resulted in differences by a factor of 2 in its quality factor.[3,8] One may expect even more prominent effects of the processing regimes on the properties of zinc niobates ($ZnNb_2O_6$) because of the possible zinc loss during sintering. In the magnesium niobates ($MgNb_2O_6$), in which only a negligible Mg evaporation is expected at sintering temperatures of around 1300°C, an increase in the annealing time of up to 50 h resulted in a noticeable improvement (by 20%) in the magnitude of the Q-factor.[3] Moreover, the authors of this study have found a significant increase in Q of the columbites with the compositions slightly deviated from stoichiometry.[8,9] More recently, all of the data on the columbites' properties have been summarized in a comprehensive review denoting a substantial variation in their Q-factor magnitudes.[10] However, the reasons for the above listed phenomena have not yet been reported. Nevertheless, from the available data it is evident that even slight structural changes may result in a significant variation of the properties of columbite niobates. One may only assume that the observed variations in the properties of columbite-based materials originate from both "extrinsic" and "intrinsic" factors. The so-called extrinsic factors comprise various materials' inhomogeneities (porosity, lattice defects, etc.), which derive from the processing. With increasing measuring frequency, their contribution to dielectric loss becomes less important compared to that of the intrinsic sources, which are determined by the crystal structure and which are proportional to frequency and permittivity.[11] In this connection, by measuring the dielectric loss over the wide frequency range beginning from centimeter waves up to the millimeter and even the submillimeter wavelength band, it is possible to evaluate and separate the respective contributions of every source to the total loss.[12] One of the simplest and most efficient ways to characterize materials in the millimeter and submillimeter wavelength bands is the use of whispering gallery mode (WGM) dielectric resonators.[13] When properly designed, the quality factor of such resonators is determined only by the dielectric properties of the material.[14,15] The WGM technique may hence give a general correlation between the defects and properties of a material, while different types of lattice inhomogeneities could be distinguished by positron lifetime spectroscopy.[16] However, to the best of our knowledge, there are no published experimental results on positron measurements of Mg, Co, and Zn columbites.

Therefore, the aim of this work was to define and estimate different structural aspects responsible for the MW dielectric loss in the nonstoichiometric columbites $A^{2+}_{1+x}Nb_2O_6$ (A^{2+} = Mg, Co, Zn).

Experimental

The ceramics with compositions $A^{2+}_{1+x}Nb_2O_6$ (A^{2+} = Mg, Co, Zn) were produced by a conventional mixed-oxide route. The starting reagents were extra-pure MgO, ZnO, Co_3O_4 (99.95%), and Nb_2O_5 (99.9%). The weighted mixtures of starting oxides were mixed in water for 4 h by vibratory mill. Then dried powders were calcined at 1100°C (A^{2+} = Zn, Co) and 1200°C (A^{2+} = Mg) for 4–8 h. After calcination, the powders were ballmilled again and pressed into disk-shaped pellets. The sintering was performed under different conditions (to eliminate the effect of material loss) in both air (8 h) and oxygen atmospheres (10 atm and 4 h) at temperatures around 1300°C (A^{2+} = Zn) and 1400°C (A^{2+} = Mg, Co). The phase composition and crystal lattice parameters of the sintered ceramics were examined by X-ray diffraction (XRD) analysis on the diffractometer DRON-3M (Burevestnik, Russia) with Cu Kα radiation.

Microstructural analysis of the ceramic samples was performed by scanning electron microscope (SEM) (JEOL, JSM 5800, Tokyo, Japan) using energy-dispersive X-ray spectroscopy (EDS) and the

* Electrochemical Society Active Member.
z E-mail: belous@ionc.kar.net; ovcharoleg@yahoo.com

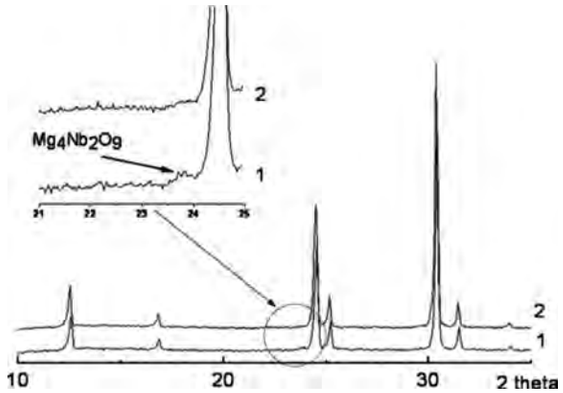

Figure 1. XRD patterns of the mixture MgO–Nb_2O_5 after firing at 1200°C for (1) 2 and (2) 6 h.

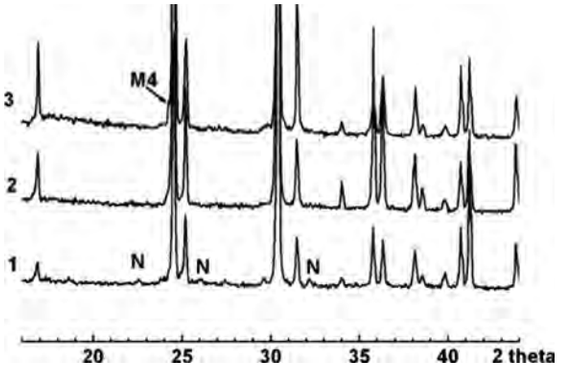

Figure 2. XRD patterns collected on the sintered $Mg_{1+x}Nb_2O_{6+x}$ samples with (1) $x = -0.03$, (2) $x = 0$, and (3) $x = 0.03$; N is Nb_2O_5 and M4 is $Mg_4Nb_2O_9$.

Link software package (ISIS 3000, Oxford Instruments, Bucks, U.K.). The dielectric characteristics of the materials ε, Q, and τ_f at frequencies of around 10 GHz were examined using a cavity reflection method on a network analyzer (PNA-L Agilent N5230A). Furthermore, to separate the contributions of both extrinsic and intrinsic factors to the dielectric loss we characterized the quality factor of the studied materials within the frequency range of 50–70 GHz by the WGM technique using a millimeter wave vector analyzer model 8-350-2 (AB Millimetre, Paris, France).[17]

The defect structure was studied by positron annihilation spectroscopy (system resolution 230 ps). The experimental setup was described in Ref. 16 and thus is not provided here. A sodium-22 source was sandwiched to minimize the positron annihilation through the edges of the samples. Each recorded spectrum contained about 6×10^6 counts, and at least three spectra were collected for each pair of samples. The experimental curves were analyzed by using the PATFIT88 program.[18] After source correction and background subtraction, the spectra were decomposed into three components: The first (τ_1) was the so-called "reduced bulk lifetime," the second (τ_2) contained information about defects inside the samples, and the third (τ_s) is responsible for the positron annihilation on the surface of the samples. This last component depended on the surface state and the position of the sodium source relative to the center of the samples and is not considered in the further discussion.

Results and Discussion

Synthesis and microstructure of the columbites $A^{2+}_{1+x}Nb_2O_{6+x}$ *(*A^{2+} *= Mg, Co, Zn).*— The peculiarities of the synthesis of the studied columbites with both stoichiometric and nonstoichiometric nominal compositions derive from the different sizes of the A^{2+} ions, their different tendencies to evaporate at sintering temperatures, and the intermediate phases that form along the calcination and sintering processes. Here, we discuss the formation of the $A^{2+}_{1+x}Nb_2O_{6+x}$ compounds in descending order with respect to the evaporation of the A^{2+} ion beginning with the Mg-based columbites.

According to the XRD data, the interaction between the oxides MgO and Nb_2O_5 starts at around 700°C with the formation of the columbite $MgNb_2O_6$, though at higher temperatures (900–1200°C) this process is accompanied by the formation of corundum-type $Mg_4Nb_2O_9$. The residual $Mg_4Nb_2O_9$ is the main problem in getting a single-phase columbite $MgNb_2O_6$ even at sintering temperature.[4,7] To avoid it, one should use both higher calcination temperatures and longer soaking times. In fact, after firing the starting mixture at 1200°C for 6 h (according to the XRD data) the product indeed contains only the single-phase $MgNb_2O_6$, as evident from Fig. 1. These data indicate that single-phase $MgNb_2O_6$ can only be synthesized provided that the appropriate calcination temperature (above 1100°C) and soaking time (6–8 h) are chosen.

In the materials $Mg_{1+x}Nb_2O_{6+x}$ sintered in air, the phase composition strongly depends on the Mg concentration. For a Mg deficiency ($x < 0$), XRD patterns demonstrate the presence of the secondary phase close to Nb_2O_5 (Fig. 2, curve 1). These data are also confirmed by electron microscopy (Fig. 3a and b).

For a Mg excess ($0 < x$), according to the crystal structure, the compositions $Mg_{1+x}Nb_2O_{6+x}$ correspond to Nb-deficient magnesium niobates $MgNb_{2-y}O_{6-5y/2}$ (where $y = 2x/x + 1$). When $0 \leq x < 0.03$, the XRD analysis indicates the presence of only matrix phase $MgNb_2O_6$ (Fig. 2, curve 2). The further increase in the Mg concentration results in the formation of a secondary Mg-rich phase

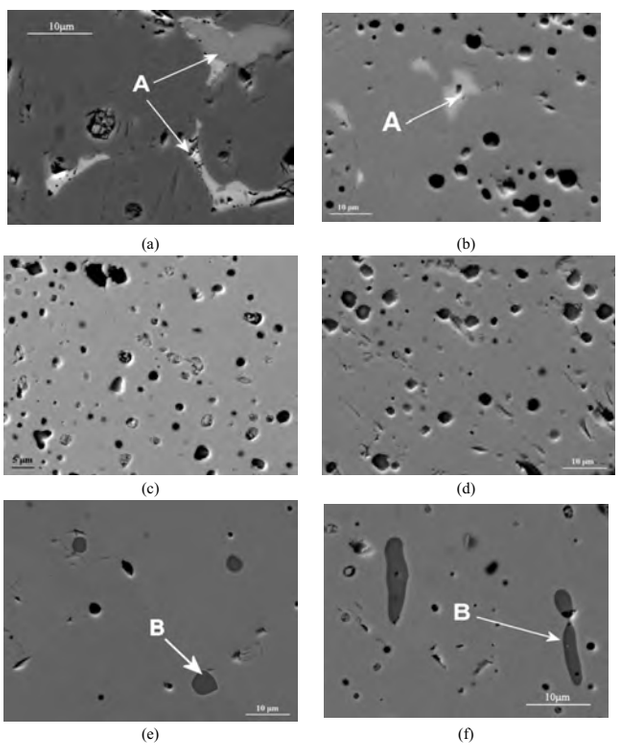

Figure 3. SEM microphotographs collected on the polished surface of the sintered columbites $Mg_{1+x}Nb_2O_{6+x}$ for (a) $x = -0.03$, (b) $x = -0.01$, [(c) and (d)] $x = 0$, and [(e) and (f)] $x = 0.03$; photographs (a), (b), (c), and (e) were developed from the samples sintered in air, whereas (d) and (f) correspond to the sintering at 10 atm oxygen pressure. A is Nb_2O_5 and B is Mg-rich phase ($Mg_4Nb_2O_9$).

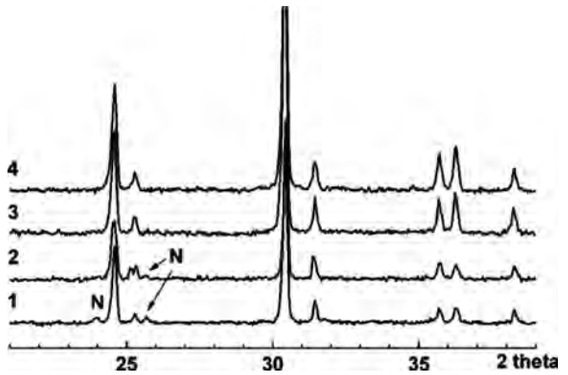

Figure 4. XRD patterns collected on the sintered $Co_{1+x}Nb_2O_{6+x}$ samples with (1) $x = -0.05$, (2) $x = -0.03$, (3) $x = 0.01$, and (4) $x = 0.03$; N is Nb_2O_5.

(Fig. 2, curve 3), which is clearly visible under SEM (Fig. 3e). Though the correct chemical composition of this Mg-rich phase is rather difficult to determine by EDS analysis, one should take into account the only stable phases, $MgNb_2O_6$ and $Mg_4Nb_2O_9$, in the $MgO–Nb_2O_5$ system that exist at room temperature.[19] Therefore, one may assume that the additional phase observed at $x \geq 0.03$, which differs from the matrix $MgNb_2O_6$ by a higher MgO content, obviously corresponds to the $Mg_4Nb_2O_9$. This phase has a corundum-like structure and demonstrates extremely high values of the *Q*-factor at MW frequencies.[20]

The sintering under 10 atm oxygen pressure did not result in any noticeable changes in the materials' microstructure, and the single-phase $MgNb_2O_6$ was again obtained for $0 \leq x < 0.03$. Similar to the samples sintered in air, those sintered in the oxygen atmosphere demonstrated a two-phase composition with a higher Mg content (Fig. 3e and f). Though the changes in the phase composition of the $Mg_{1+x}Nb_2O_{6+x}$ ceramics are quite predictable regardless of the sintering atmosphere, one important fact evident from the SEM microphotographs is the observed suppression of porosity with the increasing Mg concentration (Fig. 3e and f vs Fig. 3c and d, respectively).

In contrast to the Mg columbite, $CoNb_2O_6$ already starts to form at 600°C, which is about 100°C lower than for $MgNb_2O_6$. The formation mechanism for this compound is quite similar to that described for $MgNb_2O_6$. The only difference is that all of the reactions take place at lower temperatures.[8] Because of this feature, a single-phase Co columbite can be easily obtained even after short-term firing for 1–4 h at 1050–1100°C (Fig. 4).

Similar to the Mg columbites, the nonstoichiometric $Co_{1+x}Nb_2O_{6+x}$ with a slight Co deficiency ($x < 0$) always contains the secondary phase Nb_2O_5 (Fig. 4 and 5). However, for $x > 0$ (niobium deficiency) the different evolution of the phase composition with x is observed depending on the sintering atmosphere. Sintered in air materials $Co_{1+x}Nb_2O_{6+x}$ ($CoNb_{2-y}O_{6-5y/2}$) demonstrate a homogeneity region at $0 \leq x \leq 0.01$, which is narrower compared to that found in Mg-containing columbites. When $x > 0.01$, the small inclusions of a secondary Co-rich phase appear within the columbite matrix (Fig. 5e). The EDS analysis of this secondary phase shows that its composition is close to CoO. The Co-rich secondary phase (CoO) appears at even much lower Co concentrations

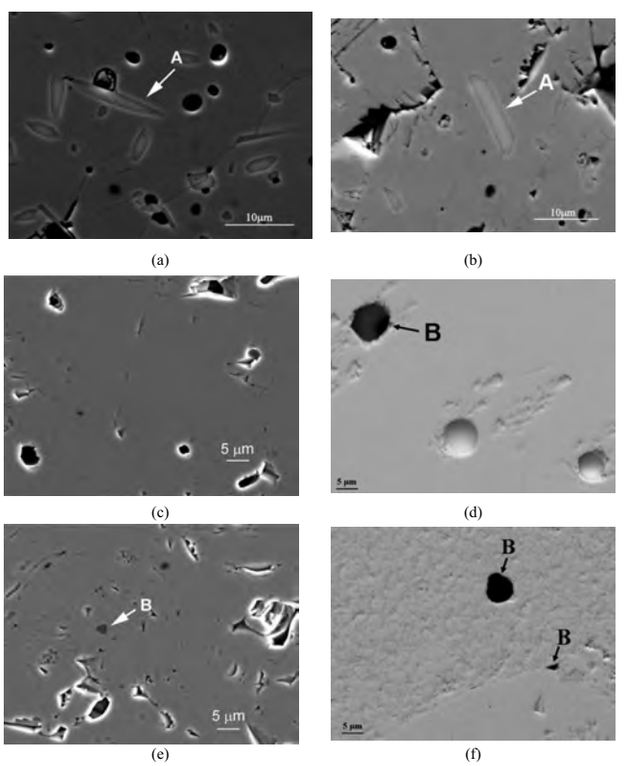

Figure 5. SEM microphotographs of the polished surfaces of the sintered columbites $Co_{1+x}Nb_2O_{6+x}$ for (a) $x = -0.03$, (b) $x = -0.01$, [(c) and (d)] $x = 0$, and [(e) and (f)] $x = 0.03$. A is the Nb-rich phase (probably Nb_2O_5) and B is the Co-rich phase (CoO). Photographs (a), (b), (c), and (e) were developed from the samples sintered in air, whereas (d) and (f) correspond to the sintering at 10 atm oxygen pressure.

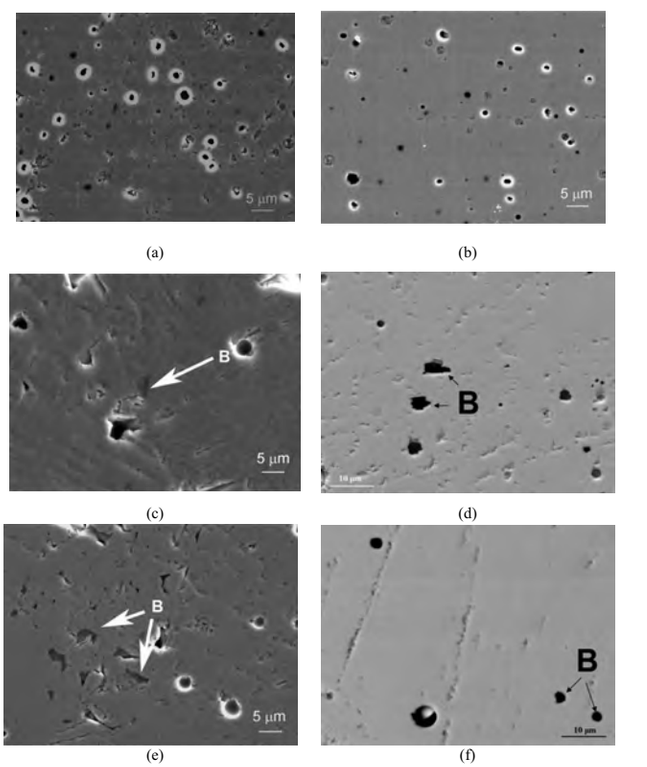

Figure 6. SEM microphotographs collected from the polished surfaces of the sintered columbites $Zn_{1+x}Nb_2O_6$ for (a) $x = 0$, (b) $x = 0.005$, [(c) and (d)] $x = 0.01$, and [(e) and (f)] $x = 0.04$. B is the Zn-rich phase ($Zn_3Nb_2O_8$). Photographs (a), (b), (c), and (e) were developed from the samples sintered in air, whereas (d) and (f) correspond to the sintering at 10 atm oxygen pressure.

Table I. Lifetime components obtained from the experimental spectra collected from the columbites sintered in air.

Material	x	τ_1 ($\pm$1) (ps)	τ_2 ($\pm$10) (ps)	I_1 ($\pm$0.5) (%)	I_d ($\pm$1) (%)
$Mg_{1+x}Nb_2O_{6+x}$	0	173	365	90	8
	0.01	176	415	91	8
	0.03	178	420	90	8
$Co_{1+x}Nb_2O_{6+x}$	0	167	412	95	3
	0.01	163	365	94	5
	0.03	169	426	95	3
	0.04	172	446	94	5
$Zn_{1+x}Nb_2O_{6+x}$	0	172	392	93	5
	0.01	171	404	94	4
	0.03	175	429	96	3

($0 \leq x$) when the materials are sintered in an oxygen atmosphere, as clearly shown in Fig. 5d and f. In contrast to the Mg-containing columbites, the sintering of cobalt niobates $Co_{1+x}Nb_2O_6$ under oxygen pressure generally results in a noticeable improvement of the microstructure of the ceramics, which becomes less porous even at higher Co concentrations (Fig. 5d and f), though containing a relatively higher amount of CoO inclusions. The latter may be associated with the suppression of the CoO evaporation under the oxygen pressure.

In contrast to the other studied columbites, $ZnNb_2O_6$ is formed by the direct interaction between zinc and niobium oxides without the formation of any secondary intermediate phases. The temperature ranges in this process are much lower compared to those of Mg- and Co-containing columbites: $ZnNb_2O_6$ starts to form at 500°C, whereas at 800°C the studied mixtures only contain a single-phase columbite.

Similar to other columbite members, when $x < 0$ the ceramics $Zn_{1+x}Nb_2O_{6+x}$ always contain a secondary phase Nb_2O_5. For $x > 0$ (niobium deficiency), regardless of the sintering atmosphere, a single-phase composition is observed for $0 \leq x \leq 0.005$. When $x > 0.005$, a Zn-rich secondary phase is formed (Fig. 6c-f). According to the EDS analysis, the composition of this phase is close to $Zn_3Nb_2O_8$, which is consistent with the previous investigations on the ZnO–Nb_2O_5 phase diagram.[21] Microstructural analysis of the columbites $Zn_{1+x}Nb_2O_{6+x}$ indicates that the increase in the zinc content in the nominal composition is accompanied by a reduced porosity of the sintered material (Fig. 6). Furthermore, sintering under oxygen pressure also improves the densification, though at the same time more secondary Zn-rich phase is formed (Fig. 6c and d).

Positron lifetime spectroscopy of the columbites $A^{2+}_{1+x}Nb_2O_{6+x}$ (A^{2+} = Mg, Co, Zn).— To examine the presence of different types of lattice defects that can arise from the compositional nonstoichiometry in the polycrystalline materials $A^{2+}_{1+x}Nb_2O_{6+x}$ (A^{2+} = Mg, Co, Zn), we used positron lifetime spectroscopy. The experimentally obtained lifetime components and their intensities collected from the columbites sintered in air are presented in Table I. After source correction and background subtraction two main components were distinguished in the spectra including the reduced bulk lifetime (τ_1), and the "defect lifetime" (τ_2) (Table I). The intensity of the first component is more than 90% for all studied samples, which suggests that either all positron annihilation occurs in the bulk of the sample (in this case τ_1 represents the bulk lifetime) or there is one more component to be separated in the spectrum that contributes to the first component. To resolve this, theoretical simulations have been performed for the $A_{1+x}Nb_2O_{6+x}$ samples (where A = Mg, Co, and Zn) with the use of the Mika program obtained from the Helsinki University of Technology to calculate lifetimes in bulk materials and in different kinds of defects. The results of the calculations are presented in Table II.

The first part of Table II contains positron lifetimes calculated in local density approximation (LDA). It can be seen that cobalt columbite has the smallest bulk lifetime (145 ps) vs the magnesium one having τ_b = 150 ps. It has been reported that the LDA underestimates the value of positron lifetime in solids.[22] At the same time, the generalized gradient approximation (GGA) gives results that agree with the experiment.[22] Comparing τ_1 from Tables I and II, one can conclude that the first component of the experimental decomposed spectrum is very close to the bulk value.

As shown in Table II, positrons are insensitive to the oxygen defects but are localized in A-type and Nb vacancies. The difference between τ_b and $\tau_A(\tau_{Nb})$, however, is less than 50 ps (Table II). This could be why it was not possible to introduce an additional component into the decomposed spectrum. If there are any defects inside of the grains, their concentration is too small to be evaluated by the positron annihilation.

At the same time, positrons are sensitive not only to the vacancies inside of the grains but also to the grain boundaries. Hübner et al. theoretically calculated the fraction of the positrons that annihilate at the boundaries depending on the grain size.[23] From Table I, one can see that the intensity of the second component (τ_2) varies from 3 up to 8%. According to Ref. 23, this can be associated with the trapping of positrons at the grain boundaries, which generally represent the highest concentration of defects and hence may give a strong influence on the positron lifetimes. Again, the fraction of positrons that annihilate at the boundaries must depend on the grain size.[23] In fact, the observed increase in the intensity of the (τ_2) component coincides well with the observed (by electron microscopy) decrease in the grain size from 5 to 8 μm for Co- and Zn-containing columbites down to 2–5 μm for the Mg-containing analogs sintered in air. Therefore, the second component in the

Table II. Results of theoretical simulations of the positron lifetimes for the annihilations in the bulk (τ_b) of the samples $A^{2+}_{1+x}Nb_2O_{6+x}$ and in different types of lattice defects.

	$Mg_{1+x}Nb_2O_{6+x}$	$Zn_{1+x}Nb_2O_{6+x}$	$Co_{1+x}Nb_2O_{6+x}$
Boronski–Nieminen enhancement factor, LDA			
τ_b (ps)	150.6	147.0	145.6
τ_O (ps)	152.6	147.4	147.0
τ_A (ps)	183.9	179.6	181.5
τ_{Nb} (ps)	175.0	172.0	172.2
Arponen–Pajanne enhancement factor, GGA			
τ_b (ps)	177.3	176.5	172.6
τ_O (ps)	180.6	177.2	174.8
τ_A (ps)	228.5	222.9	226.1
τ_{Nb} (ps)	218.6	215.6	214.9

Table III. MW dielectric properties of the columbites $Mg_{1+x}Nb_2O_{6+x}$. The materials sintered in oxygen atmosphere are marked by an asterisk. NA, not applicable.

x	Phase composition	ε (10 GHz)	τ_f (10 GHz) (ppm/C)	$Q \times f$ (10 GHz) (GHz)	$Q \times f$ (70 GHz) (GHz)
−0.03	$MgNb_2O_6$, Nb_2O_5	19.9	−56	600	NA
−0.01	$MgNb_2O_6$, Nb_2O_5	19.8	−59	1,400	NA
0	$MgNb_2O_6$	19.4	−55	58,000	47,000
0*	$MgNb_2O_6$	19.9	−60	48,000	46,000
0.01	$MgNb_2O_6$	19.9	−58	108,000	112,000
0.01*	$MgNb_2O_6$	19.3	−60	101,000	113,000
0.03	$MgNb_2O_6$, $Mg_4Nb_2O_9$	21.0	−60	121,000	113,000
0.03*	$MgNb_2O_6$, $Mg_4Nb_2O_9$	20.5	−62	112,000	117,000

decomposed spectra (τ_2) can be attributed to the annihilation in the grain boundaries. As shown in Table I, there is a consistent tendency of the component τ_2 to increase with x (increasing Nb deficiency) in $A^{2+}_{1+x}Nb_2O_{6+x}$ series. This denotes the increasing fraction of the grain boundaries in the Nb-deficient polycrystalline columbites, which agrees well with the above presented SEM results, showing an enhanced densification of the ceramics $A^{2+}_{1+x}Nb_2O_{6+x}$ with increasing x. Generally the τ_2 demonstrated a slight tendency to increase when the samples were sintered in the oxygen atmosphere.

MW characterization of the columbites $A^{2+}_{1+x}Nb_2O_{6+x}$ (A^{2+} = Mg, Co, Zn).— The MW dielectric properties of the columbites $Mg_{1+x}Nb_2O_{6+x}$ are summarized in Table III. Within the studied concentration range, a slight deviation from stoichiometry does not practically influence the dielectric constant (ε), which varies between 19 and 20. The temperature coefficient τ_f lies within the range of −55 to −60 ppm/C for all the studied compositions. At the same time, the presence of residual Nb_2O_5 at $x < 0$ is accompanied by a significant reduction in the product Qxf: The higher the amount of secondary Nb_2O_5, the lower the product Qxf is.

In stoichiometric $MgNb_2O_6$ ($x = 0$) the measured product Qxf is lower compared to that reported elsewhere.[1,3]. This may be associated with the different starting reagents and sintering temperature used in this study. In positive x values ($0 \le x < 0.03$), the magnitude of the product Qxf increases with x by 200–300% (Fig. 7, curve 1) and reaches $Qxf \approx 120{,}000$ GHz at $x = 0.03$. At $x = 0.03$ (when the highest Qxf value is observed) the materials may contain a small amount of the secondary phase $Mg_4Nb_2O_9$ with a permittivity $\varepsilon = 12$ and very high Q-factor (Qxf=210,000 GHz).[20] However, due to a low concentration of $Mg_4Nb_2O_9$ in the matrix $Mg_{1+x}Nb_2O_{6+x}$ (Fig. 3e and f), its contribution to the resulting Q-factor of a material seems to be negligible. Sintering at 10 atm oxygen pressure does not result in any noticeable changes in the magnitude and behavior of the product Qxf (Table III, Fig. 7) due to a rather low evaporation of Mg at sintering temperatures. Therefore,

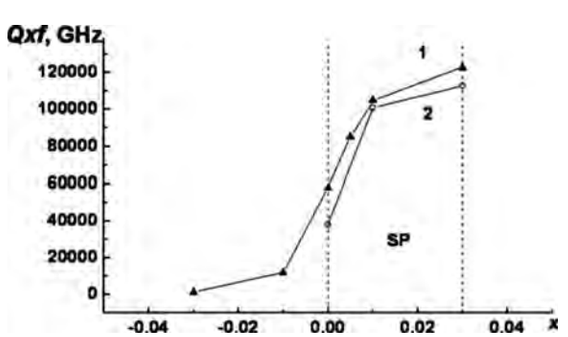

Figure 7. The product Qxf measured at 10 GHz for the columbites $Mg_{1+x}Nb_2O_{6+x}$ sintered (1) in air and (2) in oxygen at 10 atm. SP means a single-phase region.

the noticeable increase in the product Qxf with x observed in $Mg_{1+x}Nb_2O_{6+x}$ materials is most likely due to the improvement of the ceramics' microstructure associated with the reduced porosity evident from the SEM examination (Fig. 3). The lattice vacancies introduced by a slight Nb deficiency in the nominal composition of the columbite may act as the inhibitors of the grain growth, facilitating the formation of a dense structure with a high fraction of grain boundaries, which is evident from the above presented positron annihilation studies.

As clearly shown in Table III, the magnitude of the product Qxf of the magnesium niobate does not significantly change with frequency. The results measured at around 70 GHz by the WGM technique are quite similar to those obtained at 10 GHz from $TE_{01\delta}$-mode resonators. This denotes a rather low contribution of the extrinsic sources into the total value of the MW dielectric loss of Mg-containing columbites because the presence of a residual high-Q phase $Mg_4Nb_2O_9$ does not increase losses in the centimeter wavelength band (10 GHz). Therefore, the measured product Qxf is almost equal to its maximum value.

In Co columbites $Co_{1+x}Nb_2O_{6+x}$ (similar to the Mg-containing analogs), both ε and τ_f vary only slightly within the studied range of x. At the same time, the magnitude of the product Qxf depends strongly on x (Table IV, Fig. 8). At $x < 0$ the product Qxf is mainly determined by the presence of Nb_2O_5, leading to a noticeably sharp decrease in Q, whereas at $x > 0$ it is affected by two competing factors: With an increasing x an improvement of the materials' microstructure is observed, whereas it is accompanied by the formation of a secondary Co-rich phase (CoO). The latter obviously results in a decrease in Q (Table IV, Fig. 8a). When the materials are sintered under oxygen pressure, the amount of the secondary Co-rich phase is relatively higher compared to that found in the air-sintered columbites (Fig. 5d and f). Because of this, the samples sintered in oxygen never demonstrate Qxf values in the centimeter wavelength band as high as those observed in the analogs sintered in air. Therefore, the magnitude of the Q-factor reaches maximum values ($Qxf > 80{,}000$ GHz) at $x = 0$ when no secondary CoO is observed.

WGM characterization of the Co columbites at frequencies of around 60 GHz demonstrates a rather different behavior of the product Qxf with the compositional changes (Fig. 8b). The samples sintered in oxygen (when materials contain more CoO) exhibit a much higher Qxf compared to those measured in air-sintered materials at 10 GHz. Moreover, the maximum values of the Qxf are observed in the nonstoichiometric columbites ($x = 0.01$). These data indicate a suppressed contribution of the secondary Co-rich phase into the dielectric loss in the millimeter wavelength band. In this case the prevailing factor responsible for the increase in the Q-factor is the improved microstructure.

In Zn-containing columbites, both ε and τ_f vary again only slightly within the studied range of x (Table V). At the same time, the product Qxf demonstrates a behavior very similar to the Co-containing analogs (Table V, Fig. 9), which is again affected by two competing factors: an improved microstructure that is observed with an increasing x and the influence of a secondary Zn-rich phase

Table IV. MW dielectric properties of sintered columbites $Co_{1+x}Nb_2O_{6+x}$. The materials sintered in oxygen atmosphere are marked by an asterisk.

x	Phase composition	ε (10 GHz)	τ_f (10 GHz) (ppm/C)	Qxf (10 GHz) (GHz)	Qxf (70 GHz) (GHz)
−0.03	$CoNb_2O_6$, Nb_2O_5	20.2	−72	3,500	
0	$CoNb_2O_6$	20.5	−70	81,000	71,400
0*	$CoNb_2O_6$, Co-rich phase	20.0	−64	46,000	39,000
0.005	$CoNb_2O_6$	20.5	−65	75,000	65,000
0.005*	$CoNb_2O_6$, Co-rich phase	20.0	−62	45,000	95,000
0.01	$CoNb_2O_6$	20.9	−65	59,000	63,000
0.01*	$CoNb_2O_6$, Co-rich phase	20.5	−60	75,000	114,000
0.03	$CoNb_2O_6$, Co-rich phase	21.0	−65	38,000	81,000
0.03*	$CoNb_2O_6$, Co-rich phase	20.4	−60	30,000	65,000
0.04	$CoNb_2O_6$, Co-rich phase	22.0	−67	38,000	88,000
0.04*	$CoNb_2O_6$, Co-rich phase	21.2	−65	30,000	53,500

($Zn_3Nb_2O_8$). The data obtained at 10 GHz indicate that the magnitude of the Qxf product passes through the maximum at $x = 0.01$ in the materials sintered in air. The presence of the Qxf maximum may be associated with the denser structure of zinc niobate at $x = 0.01$ (Fig. 6). The effect of the secondary Zn-rich phase on the Qxf product is much weaker compared to that observed in the Co columbites because $Zn_3Nb_2O_8$ has a Qxf magnitude of around 40,000 GHz.[24] Hence, only a slight decrease in the Q-factor of a composite ceramic is observed with increasing Zn content (Fig. 9a).

In contrast, in the materials sintered under 10 atm oxygen pressure the magnitude of the Qxf product does not practically change within the studied concentration ranges due to the suppressed Zn loss. In this case the stoichiometric $ZnNb_2O_6$ sintered in the oxygen atmosphere has a much higher Q-factor (Qxf = 100,000 GHz) compared to that of the samples sintered in air.

The millimeter wave characterization of the $Zn_{1+x}Nb_2O_{6+x}$ samples sintered in air denotes a relatively weak dependence of the product Qxf on x, contrary to the measurements at 10 GHz. The observed values of Qxf are of the order of the highest Qxf observed at 10 GHz, confirming the suppression (at the millimeter wavelengths) of the "extrinsic" losses, for instance, caused by the presence of a Zn-rich phase. The samples sintered in the oxygen atmosphere demonstrate a stronger decrease in Q with x (Fig. 9b) because of the higher concentration of the secondary Zn-rich phase (Fig. 6d and f).

Conclusions

The microstructure, phase composition, and the MW quality factor of the columbites $A^{2+}_{1+x}Nb_2O_{6+x}$ (where A^{2+} = Mg, Co, Zn) are to a large extent affected by a deviation from its compositional stoichiometry. The deficiency in A^{2+} ions in the $A^{2+}_{1+x}Nb_2O_{6+x}$ ceramics always results in the formation of the secondary Nb_2O_5 phase, which significantly deteriorates the MW quality factor of sintered material. In contrast, the deficiency in Nb results in a more complicated effect. It noticeably improves the microstructure of the ceramics suppressing the associated dielectric loss in the MW region.

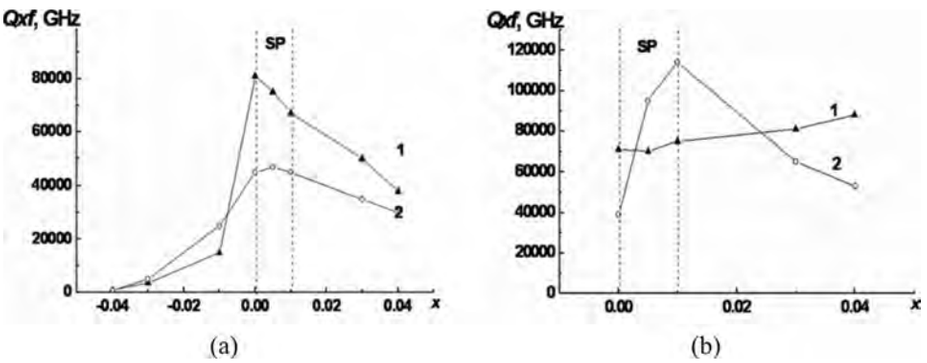

Figure 8. The product Qxf measured at (a) 10 and (b) 60 GHz for the columbites $Co_{1+x}Nb_2O_{6+x}$ sintered (1) in air and (2) in oxygen at 10 atm. SP means a single-phase region.

Table V. MW dielectric properties of sintered columbites $Zn_{1+x}Nb_2O_{6+x}$. The materials sintered in oxygen atmosphere are marked by an asterisk.

x	Phase composition	ε (10 GHz)	τ_f (10 GHz) (ppm/C)	Qxf (10 GHz) (GHz)	Qxf (70 GHz) (GHz)
0	$ZnNb_2O_6$	23.9	−74	81,000	110,000
0*	$ZnNb_2O_6$	23.5	−68	108,000	132,000
0.005	$ZnNb_2O_6$	22.5	−75	102,000	122,000
0.005*	$ZnNb_2O_6$	22.5	−71	101,000	98,000
0.01	$ZnNb_2O_6$, Zn-rich phase	23.8	−73	120,000	119,000
0.01*	$ZnNb_2O_6$, Zn-rich phase	23.7	−71	98,000	68,000
0.03	$ZnNb_2O_6$, Zn-rich phase	23.0	−71	92,000	113,000
0.03*	$ZnNb_2O_6$, Zn-rich phase	23.7	−71	110,000	83,000
0.04	$ZnNb_2O_6$, Zn-rich phase	23.7	−72	87,000	112,000
0.04*	$ZnNb_2O_6$, Zn-rich phase	23.9	−72	92,000	100,000

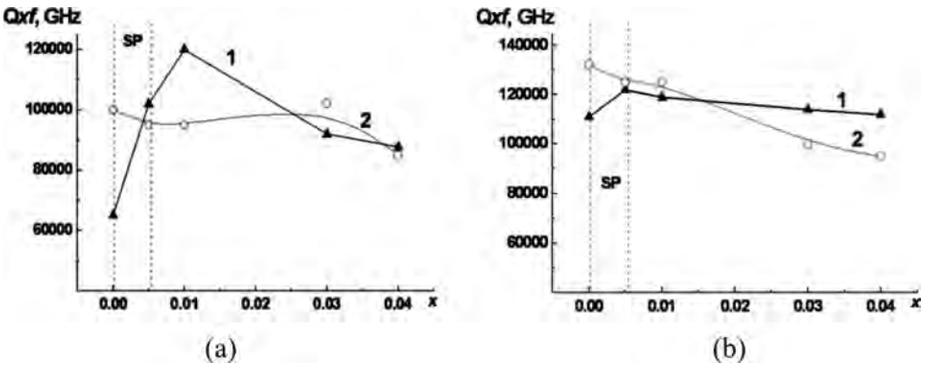

Figure 9. The product *Qxf* measured at (a) 10 and (b) 50–70 GHz for the columbites $Zn_{1+x}Nb_2O_{6+x}$ sintered (1) in air and (2) in the oxygen 10 atm. SP means a single-phase region.

However, it initiates the formation of A^{2+}-rich secondary phases ($Mg_4Nb_2O_9$, CoO, and $Zn_3Nb_2O_8$), which have a different influence on the MW quality factor depending on the A^{2+} ion. Sintering in the oxygen generally contributes to the improved densification of the polycrystalline columbites due to the stabilization of their chemical composition, though it facilitates the formation of secondary phases. As a consequence, the magnitude of the *Qxf* product of the columbites is determined by the competing contribution of the above listed factors and demonstrates a rather nonlinear variation with *x*. The comparison of the $Qxf(x)$ product measured at 10 and 50–70 GHz indicates a noticeable extrinsic contribution to the MW dielectric loss observed in the Co- and Zn-containing columbites, which is foremost associated with the presence of Co- and Zn-rich secondary phases in sintered materials. The contribution of these phases into the dielectric loss of a material weakens significantly with measuring frequency. In the Mg-containing columbites, this effect is negligible because the dielectric loss of the corresponding secondary phase $Mg_4Nb_2O_9$ is less than that of the columbite matrix. As a result of the careful choice of both the chemical compositions within the $A^{2+}_{1+x}Nb_2O_{6+x}$ series and the sintering atmospheres, a promising MW dielectrics with a *Qxf* magnitude of as high as 100,000–120,000 GHz was developed.

Acknowledgments

This work was partially supported by a NATO Grant under the NATO SfP project 980881 "Dielectric Resonators" of the NATO "Science for Peace" Program. This research was also supported by the Natural Sciences and Engineering Research Council of Canada (NSERC).

References

1. H. J. Lee, K. S. Hong, S. J. Kim, and I. T. Kim, *Mater. Res. Bull.*, **32**, 847 (1997).
2. Y. C. Zhang, Z. X. Yue, Z. Gui, and L. T. Li, *Mater. Lett.*, **57**, 4531 (2003).
3. R. C. Pullar, J. D. Breeze, and N. McN. Alford, *J. Am. Ceram. Soc.*, **88**, 2466 (2005).
4. K. Sreedhar and A. Mitra, *Mater. Res. Bull.*, **32**, 1643 (1997).
5. T. Kolodiazhnyi, A. Petric, A. Belous, O. V'yunov, and O. Yanchevskij, *J. Mater. Res.*, **17**, 3182 (2002).
6. M. T. Sebastian, *Dielectric Materials for Wireless Communication*, p. 688, Elsevier Science, Oxford (2008).
7. A. Ananta, R. Brydson, and N. W. Thomas, *J. Eur. Ceram. Soc.*, **19**, 355 (1999).
8. A. Belous, O. Ovchar, O. Kramarenko, B. Jancar, J. Bezjak, and D. Suvorov, *Inorg. Mater.*, **42**, 1369 (2006).
9. A. Belous, O. Ovchar, J. Bezjak, and B. Jancar, *J. Eur. Ceram. Soc.*, **27**, 2933 (2007).
10. R. C. Pullar, *J. Am. Ceram. Soc.*, **92**, 563 (2009).
11. J. Petzelt and S. Camba, *Mater. Chem. Phys.*, **79**, 175 (2003).
12. A. K. Tagantsev, J. Petzelt, and N. Setter, *Solid State Commun.*, **87**, 1117 (1993).
13. G. Annino, D. Bertolini, M. Cassettari, M. Fittipaldi, I. Longo, and M. Martinelli, *J. Chem. Phys.*, **112**, 2308 (2000).
14. J. Krupka, *Meas. Sci. Technol.*, **17**, R55 (2006).
15. T. Kolodiazhnyi, G. Annino, and T. Shimada, *Appl. Phys. Lett.*, **87**, 212908 (2005).
16. R. Krause-Rehberg and H. S. Leipner, *Solid-State Sciences*, p. 127, Springer, Berlin (1999).
17. G. Annino, M. Cassettari, I. Longo, and M. Martinelli, *IEEE Trans. Microwave Theory Tech.*, **45**, 2025 (1997).
18. P. Kirkegaard, N. J. Pedersen, and M. Eldrup, PATFIT88, Risø National Laboratory, Denmark (1989).
19. Y. C. You, H. L. Park, Y. G. Song, H. S. Moon, and G. C. Kim, *J. Mater. Sci. Lett.*, **13**, 1487 (1994).
20. A. Kan, H. Ogawa, A. Yokoi, and H. Ohsato, *Jpn. J. Appl. Phys., Part 1*, **42**, 6154 (2003).
21. O. Yamaguchi, N. Maruyama, and K. Hirota, *J. Mater. Sci. Lett.*, **10**, 445 (1991).
22. B. Barbiellini, M. J. Puska, T. Korhonen, A. Harju, T. Torsti, and R. M. Nieminen, *Phys. Rev. B*, **53**, 16201 (1996).
23. C. Hübner, T. Staab, and R. Krause-Rehberg, *Appl. Phys. A: Mater. Sci. Process.*, **61**, 203 (1995).
24. D.-W. Kim, K. H. Ko, and K. S. Hong, *J. Am. Ceram. Soc.*, **84**, 1286 (2001).